Tetracycline absorbed onto nitrilotriacetic acid-functionalized magnetic graphene oxide: Influencing factors and uptake mechanism

Mei-fang Li [a,b], Yun-guo Liu [a,b,*], Guang-ming Zeng [a,b], Shao-bo Liu [c], Xin-jiang Hu [d,e], Ding Shu [f], Lu-hua Jiang [a,b], Xiao-fei Tan [a,b], Xiao-xi Cai [a,b], Zhi-li Yan [a,b]

[a] College of Environmental Science and Engineering, Hunan University, Changsha 410082, PR China
[b] Key Laboratory of Environmental Biology and Pollution Control (Hunan University), Ministry of Education, Changsha 410082, PR China
[c] School of Metallurgy and Environment, Central South University, Changsha 410083, PR China
[d] College of Environmental Science and Engineering, Central South University of Forestry and Technology, Changsha 410004, PR China
[e] College of Natural Resources and Environment, South China Agricultural University, Guangzhou 510642, PR China
[f] Light Alloy Research Institute, Central South University, Changsha 410083, PR China

GRAPHICAL ABSTRACT
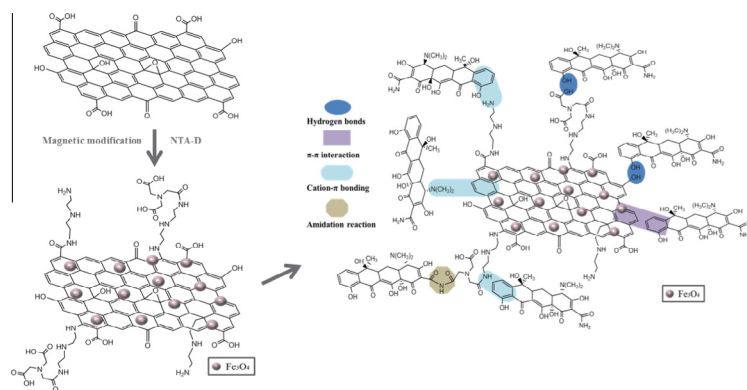
ARTICLE INFO

ABSTRACT

A novel magnetic nanomaterial was synthesized by grafting nitrilotriacetic acid to magnetic graphene oxide (NDMGO), which was applied as an adsorbent for removing tetracycline (TC) from aqueous solutions. The nanomaterial was characterized using TG-DTA, SEM, TEM, XRD, VSM, XPS, Raman, BET surface area and zeta potential measurements. Several experimental conditions (solution pH, adsorption time, temperature, ionic strength and foreign ions) affecting the adsorption process were investigated. The results showed that the TC adsorption capacity could be affected by solution pH. The adsorption capacity of TC increased rapidly in the initial 20 min and finally reached equilibrium was about 600 min. The pseudo-second-order kinetics provided the better correlation for the experiment data. Various thermodynamic parameters indicated that the adsorption was a spontaneous and endothermic process. The presence of NaCl and background electrolytes in the solution had a slight influence on TC adsorption. Hydrogen bonds, amidation reaction, π-π and cation-π interaction between NDMGO and TC could be used to explain the adsorption mechanism. The regeneration experiment demonstrated that this nanomaterial possessed an excellent regeneration performance. Based on the experimental results

* Corresponding author at: College of Environmental Science and Engineering, Hunan University, Changsha 410082, PR China.
  E-mail address: liuyunguo_hnu@163.com (Y.-g. Liu).

and comparative analysis with other adsorbents, the NDMGO was a high-efficiency and reusable adsorbent for TC pollution control.

1. Introduction

Antibiotics are increasingly being used in the world to resist disease and protect the health of humans and animals. In China, approximately 2.1×10^5 tons of antibiotics are produced per year, and 85% of which is utilized in animal agriculture and medicine [1]. Tetracycline (TC, $C_{22}H_{24}N_2O_8$), as a widely used antibiotics in the world, is used frequently in human therapy and livestock industry [2], resulting in approximately 50–80% of unmetabolized parent compounds entering into the environment [3]. In fact, large amounts of TC have been recently detected in surface water, ground water, and even drinking water [4,5], which may pose potential risks to aquatic ecological environment and human health via the endocrine disruption and promotion of antibiotic resistance genes (ARGs) transformation between nonpathogenic and pathogenic bacteria [6,7]. Consequently, it is imperative to find an efficient and feasible method to remove TC.

To date, many methods have been reported to decontaminate TC such as adsorption [8], biodegradation [9], photodegradation [10], hydrolysis and oxidative degradation [11]. Among these methods, adsorption has attracted special interest in the treatment of TC pollutants due to its accessibility, high efficiency and harmless to the environment. Various adsorbents have been applied to investigate the adsorption performance of TC, including aluminum oxide [12], clays [13], activated carbons [14], carbon nanotubes [2], and biochar [15,16]. However, these adsorbents suffer the problem of limited adsorption ability, high cost or poor regeneration performance. Hence, developing an adsorbent with high adsorption capacity, low production cost, excellent regeneration performance, and environment friendly for TC removal should be conducted and studied urgently.

Graphene oxide (GO), a two-dimensional (2D) monolayer nanomaterial of sp^2-bonded carbon atoms packed densely in a hexagonal honeycomb lattice, is considered to be a superior adsorbent due to its chemical stability, large specific surface area, rich oxygen-containing groups and feasibility of mass production [17]. Currently, owing to its unique surface structure and hydrophilicity, GO serves as a promising adsorbent for the removal of organic aromatic compounds from aqueous solutions [18], such as polycyclic aromatic hydrocarbons [19], aromatic polyketide antibiotics [20], dyes [19], chlorinated aromatic hydrocarbons [18] and phenolic compounds [21]. TC is an amphoteric polyketides consisting of naphthacene ring structure and each ring includes phenol, alcohol, ketone and amino functional groups [22]. Therefore, TC could be removed by GO, which has been demonstrated by Gao et al. [5]. However, in practical application, GO is very hard to separate and recycle from aqueous solutions after the adsorption process [23]. Consequently, novel GO composite materials are required to be synthesized to overcome this drawback and improve the adsorption performance of GO for TC pollution control. Liu et al. [24] was reported that grafting magnetic nanoparticles to GO surface could provide convenience for the solid-liquid separation, but they would take up the adsorption sites on GO surface and were unfavorable to the adsorption [25]. Many researches showed that new chemical substances containing hydrophilic groups could be introduced to enhance the adsorption ability [26,27]. Like other multidentate chelating agents, nitrilotriacetic acid (NTA) is a well-known amino-carboxylic chelating agent possessing one amide group and three carboxyl groups, which can form stable chelates with most metals [26,28]. Besides, the nitrogen-containing functional groups have a relatively high reactivity and easily react with many chemicals [29]. Therefore, NTA is found to be an ideal choice for GO surface modification applications.

In this study, a novel magnetic composite was synthesized by grafting NTA to magnetic graphene oxide (MGO) through diethylenetriamine and applied to remove TC from aqueous solutions. The objectives of this work were to (1) optimize the adsorption conditions by investigating the effects of solution pH, contact time, temperature, ionic strength and background electrolytes; (2) probe the regeneration performance of NDMGO using desorption experiment; (3) evaluate the adsorption capacity of NDMGO by comparing with other adsorbents; and (4) discuss the adsorption mechanism between TC and NDMGO based on the kinetics, thermodynamic models, FTIR and XPS analysis.

2. Experimental section

2.1. Materials

The reagents such as 1-ethyl-3-(3-dimethylaminopropyl) carbodiimide hydrochloride (EDC), N-hydroxyl succinimide (NHS) were supplied by Shanghai Civi Chemical Technology Co., Ltd. Tetracycline hydrochloride (TC) was obtained from Hefei Bomei Biotechnology Co., Ltd. Graphite powder, NTA, diethylenetriamine, $FeCl_3·6H_2O$, $FeSO_4·7H_2O$, 30% H_2O_2, 98% H_2SO_4 and some other chemicals used in the experiments were purchased from Sinopharm Chemical Reagent Co., Ltd., China. Milli-Q water was used in all experiments.

2.2. Preparation of MGO

GO was prepared via oxidizing natural graphite powder following the modification of Hummers's method [30]. The specific synthesis methods of GO have been reported in the previous research [31]. Next, the magnetic graphene oxide (MGO) was prepared by co-precipitation method [32]. Briefly, 200 mL mixed solution of Fe^{3+} ($0.1 \, mol \, L^{-1}$) and Fe^{2+} ($0.05 \, mol \, L^{-1}$) was added to the 400 mL GO suspension ($5 \, mg \, mL^{-1}$) with addition of ammonia solution at 85 °C for 45 min to form Fe_3O_4-GO composite.

2.3. Preparation of NDMGO

NDMGO was obtained by reacting NTA with MGO through diethylenetriamine. EDC (0.4 g) and NHS (0.4 g) were added to the NTA (0.8 g) solution with continuous stirring for 2 h in order to activate the carboxyl groups of NTA [28,33,34]. Then the diethylenetriamine and MGO dispersion were added and reacted at room temperature. The mixed solution was continuously stirred at 80 °C for 6 h [25,28]. The obtained product was rinsed with Milli-Q water until the solution pH was about 7.0, and then stored at room temperature. The preparation sketch of NDMGO is shown in Fig. 1.

2.4. Characterization

TG and DTA curves were measured using thermoanalytical equipment (SDT Q600, USA) in nitrogen atmosphere from 0 to 1000 °C (heating rate was $10° \, min^{-1}$). The BET specific surface area
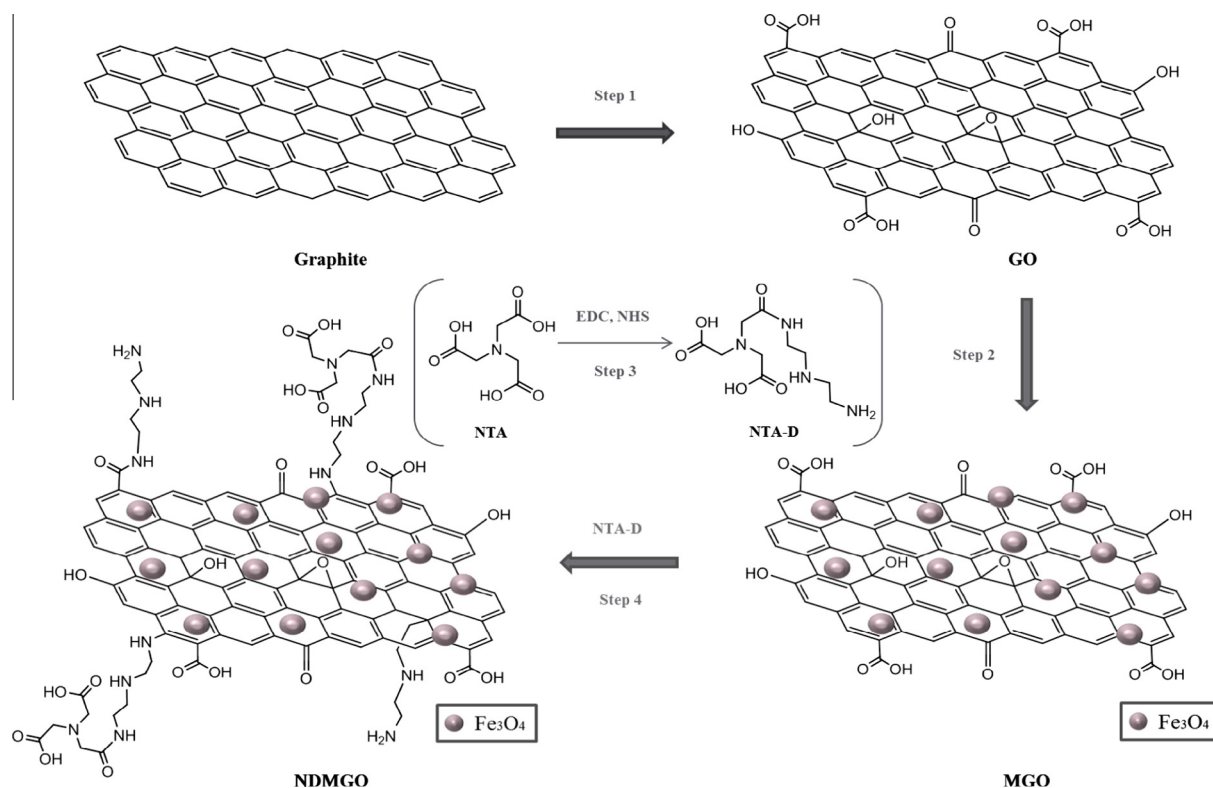
Fig. 1. Schematic depiction of the synthesis of NDMGO.

and pore structure were recorded by using nitrogen adsorption-desorption measurements (Autosorb-1, Quantachrome Instruments, USA). The cross sectional area of a nitrogen molecule used to calculate the BET specific surface area was 16.2 A^2. The structure and morphology of NDMGO were observed with scanning electron microscopy (SEM) (Hitachi S-4800, Japan) and transmission electron microscopy (TEM) (Tecnai G2 F20, USA). The FT-IR spectra of NDMGO before and after cross-linking TC were carried out by using a spectrophotometer (Nicolet 6700). The X-ray diffraction (XRD) pattern was performed with a Bruker D8-Advance X-ray diffractometer (Bruker, German). Magnetic properties were obtained on a vibrating sample magnetometer (VSM) (Lake Shore 7410, USA). The surface states of NDMGO were conducted based on ESCALAB 250Xi X-ray photoelectron spectroscopy (XPS) (Thermo Fisher, USA). The Raman spectrum was measured by using a Raman Microscope (Labram-010, JY, FAR). For the zeta potentials analysis, 9.6 mg NDMGO was added into 50 mL Milli-Q water followed by ultrasonification, and then the solution pH (2.0–11.0) was adjusted by adding negligible volumes 0.1 M NaOH or HCl. The zeta potentials of NDMGO in solution were determined by using a zeta potential meter (Zetasizer Nano-ZS90, Malvern).

2.5. Sorption experiments

A 1 g L^{-1} standard stock solution of TC used in this experiment was prepared by dissolving specific amounts of TC powder into Milli-Q water and kept in dark, because TC would direct photolysis in the presence of sunlight [2]. All batch adsorption experiments were carried out by adding 1 mL (9.6 mg mL^{-1}) NDMGO into 50 mL of TC solutions and shaken for 24 h with a shaking speed of 150 rpm at 25 °C. The desired pH values of the solutions were adjusted by adding negligible volumes of 0.01–0.1 mol L^{-1} HCl and NaOH solutions. The solid/liquid phases were separated using a magnet. The concentrations of residual TC in the supernatant were determined by an UV–Vis spectrophotometer (UV-2550, SHIMADZU, Japan) at 357 nm [20].

The effects of initial solution pH on TC adsorption were conducted at pH ranging from 2.0 to 11.0 and two different concentrations (30 and 50 mg L^{-1}, respectively). Kinetic experiments were performed by increasing the shaking time from 0 to 1440 min with 50 mg L^{-1} TC solutions. Adsorption thermodynamic studies were carried out with initial concentrations of TC between 50 and 500 mg L^{-1}, and the experimental temperatures were controlled at 283, 298, and 313 K, respectively. The effects of ionic strength were adjusted by dissolving different amount of NaCl. Four foreign ions (K$^+$, Ca^{2+}, Cl$^-$ and NO$_3^-$) were added to 10 and 50 mg L^{-1} TC solutions in order to evaluate the effects of background electrolytes on TC adsorption.

2.6. Desorption experiments

The regeneration of NDMGO was conducted by adding TC-loaded NDMGO to 0.01 M NaOH solution (500 mL). The mixture was stirred at 25 °C for 24 h. The same step was repeated for five times and the solid/liquid phases were separated using a magnet. In each cycle of adsorption, suspension liquid containing 96 mg NDMGO and 50 mg L^{-1} of TC (500 mL) was shaken at 25 °C for 24 h with pH 4.0.

The calculation formula of TC adsorption capacity (q_e) is given in the following equation:

$$q_e = \frac{(C_o - C_e)V}{m} \tag{1}$$

where C_o and C_e (mg L^{-1}) are the initial and equilibrium TC concentrations, respectively; V (L) is the initial volume of the TC solutions, and m (g) is the mass of the adsorbent used.

3. Results and discussion

3.1. Characterization of NDMGO

The TG and DSC curves of NDMGO were investigated by the thermogravimetric analysis (TGA). As shown in Fig. 2a, NDMGO presented slight weight loss (10%) between 14 and 85 °C, suggesting a dehydration process. However, the distinct weight loss (47%) appeared at 85–1000 °C, which could be ascribed to the destruction of the labile oxygen-containing functional groups such as epoxy, carboxyl and hydroxyl groups on the NDMGO. Meanwhile, the DSC curve displayed a sharp endothermic peak centered at 853 °C, indicating that some amorphous iron oxide was decomposed.

Nitrogen adsorption-desorption isotherms were carried out to characterize the specific surface areas and pore size of NDMGO (Fig. 2b). Generally, relative larger surface area of the adsorbents could achieve a better adsorption performance. The BET surface area of the NDMGO was measured to be 249 $m^2 g^{-1}$, which confirmed a larger specific surface area than that of MGO (115 $m^2 g^{-1}$) [28]. This result might be due to the introduction of NTA on the MGO. Guo et al. [28] also confirmed that the BET surface area of the adsorbent after modification was much higher than that of MGO. The pore size distribution of MGO was shown in Fig. S1. The average pore diameter of MGO and NDMGO were 1.4 and 4.3 nm, indicated that micropores and mesopores were the predominant pores for the MGO and NDMGO, respectively.
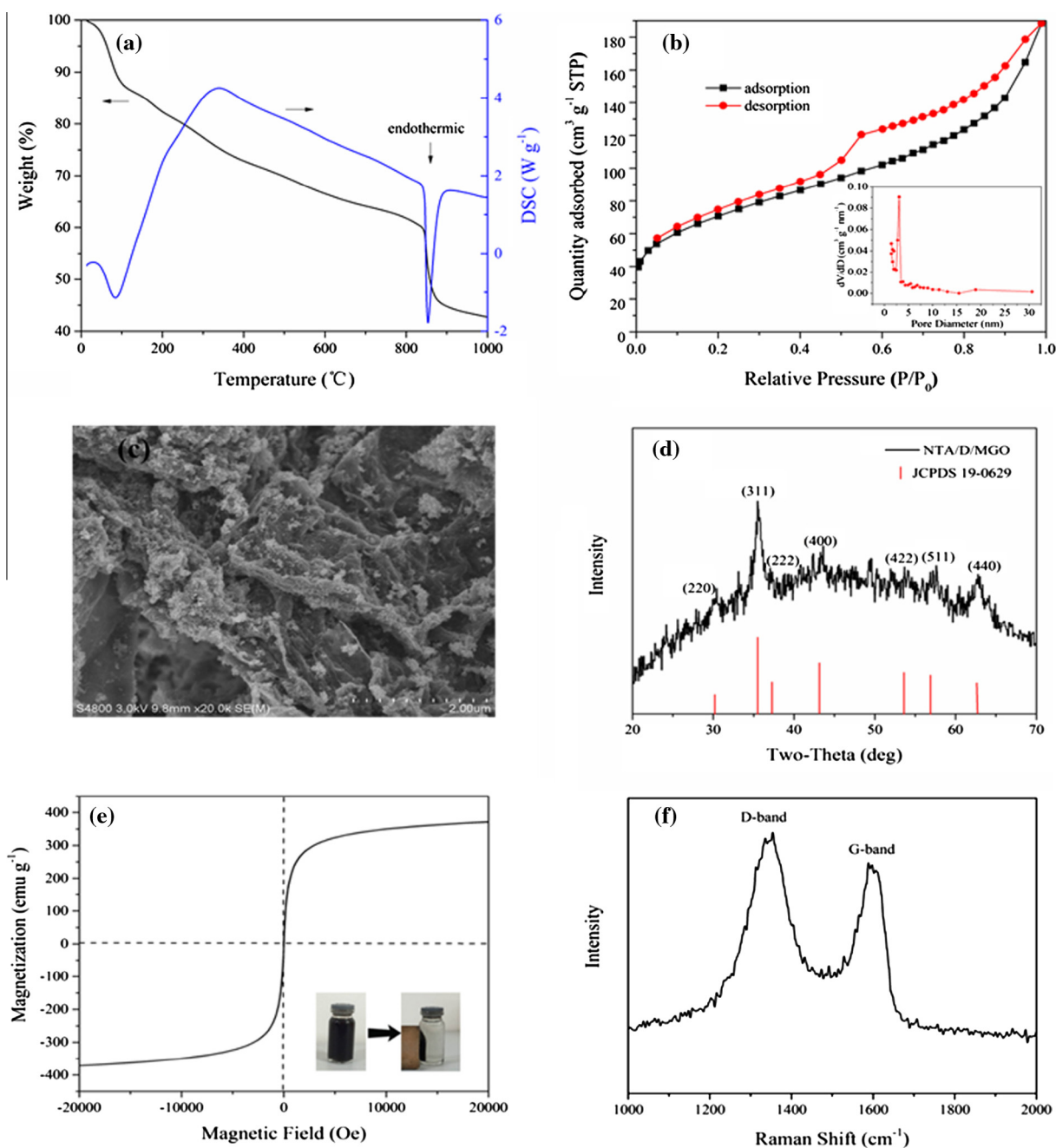

Fig. 2. Characterization of NDMGO: (a) TG-DTA curves; (b) nitrogen adsorption-desorption isotherms (the inset shows the pore size distribution of the NDMGO); (c) SEM photograph; (d) XRD pattern; (e) magnetization curve (the inset shows the NDMGO dispersed in ultrapure water and the magnetic separation); and (f) Raman spectrum of NDMGO.

The SEM image of NDMGO is illustrated in Fig. 2c. Compared with the pure GO, it was apparent that wrinkles and groove regions were primarily presented on the surface of NDMGO and formed the scrolling of GO sheets [35]. Fig. S2a shows that the NDMGO could be well dispersed in ultrapure water. The TEM image of the NDMGO (Fig. S2b) indicated that Fe_3O_4 nanoparticles were loaded on the GO nanosheets successfully. According to the XRD pattern of NDMGO (Fig. 2d), seven diffraction peaks at 30.19, 35.52, 37.05, 43.05, 53.61, 57.19 and 62.79° (2θ) were detected, which matched well with the indexed peaks of Fe_3O_4 (JCPDS 19-0629) [36]. The results revealed that NTA binding did not change the crystalline phase of the magnetic nanoparticles (Fe_3O_4).

Vibrating sample magnetometry (VSM) was employed to analyze the magnetization of NDMGO. Fig. 2e shows the hysteresis loop of NDMGO nanocomposite. The saturation magnetization of NDMGO was measured to be 371 emu g^{-1}. This value was far greater than that reported for bare Fe_3O_4 (37 emu g^{-1}) [36], demonstrating that a considerable amount of Fe_3O_4 were successfully loaded on the NDMGO surface. Fig. 2e also presented almost zero coercivity and remanence, suggesting that NDMGO showed a superparamagnetic behavior [37]. According to the inset of Fig. 2e, the NDMGO could be effectively separated using a magnet.

In the Raman spectrum (Fig. 2f), significant structural changes were occurred during the modification process from GO to NDMGO. For the NDMGO samples, two obvious peaks at 1355 and 1598 cm^{-1} corresponded to the D band and G band, respectively were observed, which were similar to the previous study about GO [25]. The D band derives from the stretching vibrations of sp^3 carbon atoms, which induces defects and disorders. However, the G band is usually related to the E_{2g} mode of sp^2 carbon domains. The increased I_D/I_G intensity ratio of NDMGO (1.2) compared with GO (0.9) implied that some structural changes had occurred due to the introduction of abundant functional groups during the modification process [38].

XPS analysis was performed on MGO before and after its reaction with diethylenetriamine and NTA (NTA-D). Fig. 3a gives the full survey scan of XPS spectra. Compared with MGO, an extra N peak was observed in the full spectra of NDMGO, which might be originated from the grafted NTA-D. To further descript the relative contents of core groups, the C1s and N1s spectra are summarized in Fig. 3b –d. The C1s peak for NDMGO could be resolved into four component peaks centered at 284.74, 285.50, 286.35, and 288.03 eV, corresponding to C—C/C=C, C—N, C—O, and C=O groups, respectively. The C1s peak for MGO included five peaks at approximately 284.75, 285.96, 286.98, 288.79, and 291.13 eV, which were attributable to C—C/C=C, C—O, C—O—C, C=O, and O—C=O groups species, respectively [23,39]. The peaks at 286.98 and 291.13 eV for NDMGO were absent, which might be ascribed to the reaction of the oxygen-containing functional groups of MGO with NTA-D. The extra N1s XPS spectrum of NDMGO is reported in Fig. 3d. The N1s peak of NDMGO showed three types of individual peaks located at 399.94, 400.14, and 403.02 eV, which were correlate to —(CH$_2$)$_3$N, —NH/C—N, and N$^+$, respectively [40–42]. The peak at 399.94 eV exhibited the possible contribution
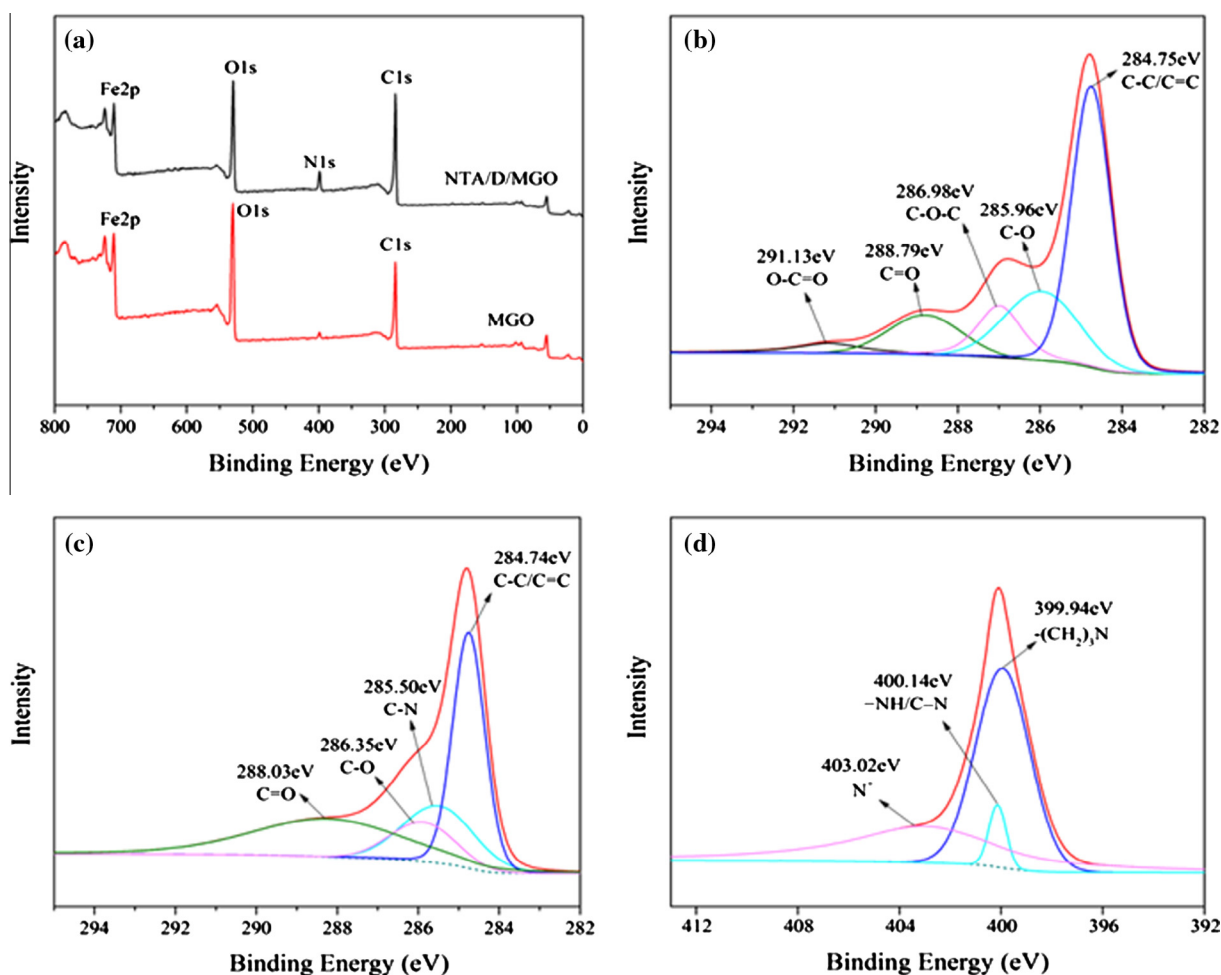

Fig. 3. (a) XPS wide-scan; (b) C1s XPS spectra of MGO; (c) C1s and (d) N1s XPS spectrum of NDMGO.

Table 1
The atomic percentages of C, N, O and Fe.

Materials	Atomic %			
	C1s	N1s	O1s	Fe2p
MGO	50.72	2.95	35.95	10.38
NDMGO	60.50	7.51	24.52	7.47

from the NTA, reflecting that the NTA molecules have been successfully coupled to the NDMGO. The atomic percentages of C, N, O and Fe were obtained from XPS characterization analysis (Table 1). The atomic ratio of C and Fe was about 5:1 after grafting magnetic nanoparticles to GO surface. When NTA-D was uploaded on the MGO, the C atom concentration was increased by about 20% and the atomic ratio of C and N was changed from 17:1 to 8:1, which further suggested that the surface of GO might be grafted a lot of nitrogen-containing groups.

3.2. Effects of pH and modification

Solution pH is a key factor affecting removal efficiency of TC by changing the surface charge of the adsorbent, the speciation distribution of the target compounds and the degree of ionization [43]. The effects of pH are shown in Fig. 4a. By increasing the solution pH values from 2.0 to 4.0, the adsorption capacity of TC on NDMGO increased. However, when the pH values were higher than 4.0, the adsorption capacity decreased with increasing of pH. Therefore, the maximum adsorption capacity could be achieved at pH around 4.0 and the values were 155 and 212 mg g^{-1}, corresponding to initial TC concentration of 30 and 50 mg L^{-1}, respectively. It could be concluded that the adsorption behavior of TC by NDMGO showed clearly pH dependence. This might be ascribed to the molecular structural characteristics of TC and various functional groups on the surface of NDMGO.

Under different acid dissociation constants (pK_a = 3.3, 7.7, and 9.7), TC exists as a cationic (TCH^{3+}), zwitterionic (TCH$_2^0$), and anionic (TCH$^-$ or TC^{2-}) species, respectively. Whereas the zeta potentials of NDMGO decreased with increasing the solution pH from 2.0 to 11.0 due to the dissociation of carboxylic group (—COOH) on the NDMGO surface (Fig. 4b). At pH < 6.2, the zeta potentials of NDMGO were positive. At pH > 6.2, the surface of NDMGO was negatively charged. Among the pH range in this experiment, the electrostatic repulsion might exist between the TCH^{3+} and positive NDMGO surface, as well as between the TCH$^-$ or TC^{2-} and negative NDMGO surface. The optimal pH should be showed at 6.2. However, the optimal pH appeared at 4.0. Hence, electrostatic attraction could not be used to explain the main mechanism of TC adsorption by the NDMGO.

In order to further test the adsorption capacity before and after modification, the 50 mg L^{-1} TC adsorption by GO at pH 2.0–11.0 and by MGO at pH 4.0 were studied and presented in
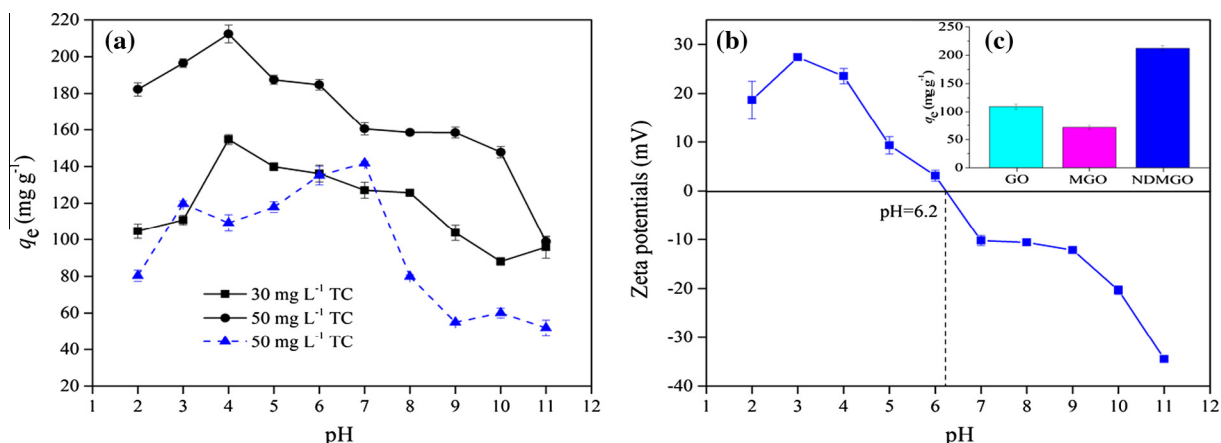

Fig. 4. (a) Effects of pH on TC adsorption: the solid lines are the NDMGO adsorption and the dotted line is the GO adsorption; (b) zeta potentials of NDMGO at different pH; (c) comparison of adsorption capacities of GO, MGO, and NDMGO for TC. m/V = 0.19 g L^{-1}, T = 25 °C, t = 24 h.
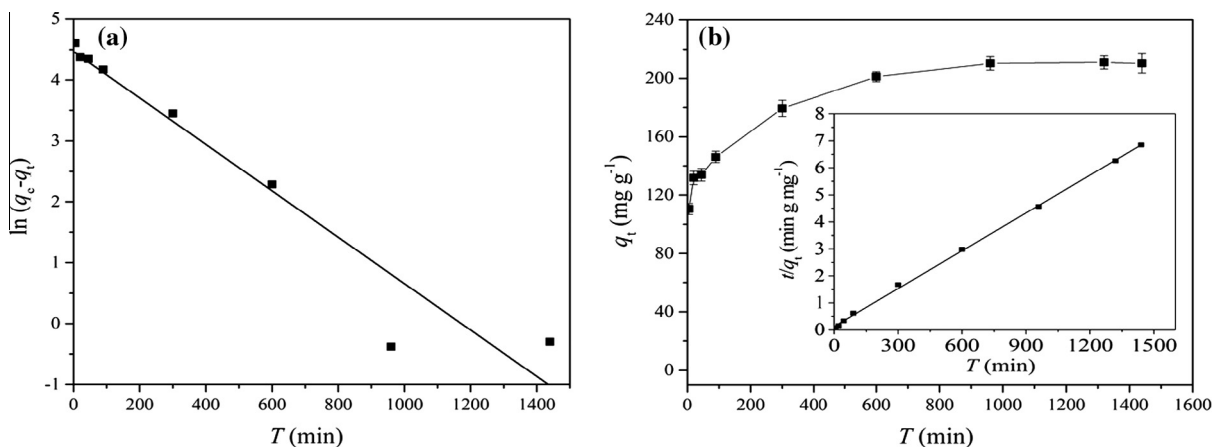

Fig. 5. (a) The pseudo-first-order kinetics model; (b) effects of contact time on the TC adsorption (the inset shows pseudo-second-order kinetics model). $C_{0(TC)}$ = 50 mg L^{-1}, m/V = 0.19 g L^{-1}, T = 25 °C, pH = 4.0.

Table 2
Kinetic parameters for TC adsorption by NDMGO.

$q_{e,exp}$	Pseudo-first-order			Pseudo-second-order		
	k_1 (min^{-1})	$q_{e,1}$ (mg g^{-1})	R^2	k_2 (g mg^{-1} min^{-1})	$q_{e,2}$ (mg g^{-1})	R^2
211	3.81×10^{-3}	87	0.924	1.65×10^{-4}	215	0.999

Fig. 4a and c. At the same TC concentration, the NDMGO always had 1.5–3 times higher adsorption capacity for TC removal than that of GO. From Fig. 4c, the TC adsorption capacity on NDMGO was measured to be 212 mg g^{-1}, which was two times higher to GO (109 mg g^{-1}) and three times higher to MGO (72 mg g^{-1}), respectively. It might due to the NDMGO contained abundant amino and carboxyl groups. As shown in Fig. 2e, the NDMGO could be easily collected with a magnet since the magnetic nanoparticles loaded on the GO sheets successfully, however, the adsorption capacity of MGO was lower than that of GO. The main reason was that some sorption sites of GO were taken up by the magnetic nanoparticles and the magnetic nanoparticles could induced the aggregation of GO [44]. These results illustrated that the material was modified successfully and the NDMGO might be an outstanding adsorbent in treating waste water contaminated by TC.

3.3. TC adsorption kinetics

The effects of the contact time on the adsorption capacity of NDMGO for TC are shown in Fig. 5. Obviously, owing to the large surface area, the high surface reactivity and the sufficient exposure of active sites of the NDMGO, the adsorption capacity of TC increased rapidly in the initial 20 min. Nevertheless, the needed time from the beginning to the adsorption equilibrium was about 600 min, which was far longer than that of GO (within 15 min) [20]. This fact might be associated with the pore structure of NDMGO. It was found that mesopores were the predominant pores for the NDMGO and the pore size of NDMGO mainly distributed at 3.0 nm (Fig. 2b). Besides, this nanomaterial also had many micropores. The diffusion resistance of TC in the micropores was greater than that in the hemocompatibility and mesopores, and relatively small mesopores sizes might also hinder the TC uptake [45]. Hence the adsorption time on TC by NDMGO was long. In order to ensure all samples reaching adsorption equilibrium, 24 h was chosen as the reaction time in the following experiments.

To understand the adsorption rate of NDMGO, the pseudo-first-order and pseudo-second-order kinetic models have been used to analyze the TC adsorption kinetics data [46]. Detailed information about these models can be found in the Supplementary materials.

The linearized fitting forms of the pseudo-first-order and pseudo-second-order models for the adsorption of TC onto NDMGO are given in Fig. 5. The kinetics parameters of the two models are summarized in Table 2. Obviously, the pseudo-second-order kinetics model in Fig. 5b showed a better regression coefficient for the kinetic data ($R^2 = 0.999$) than pseudo-first-order kinetics model in Fig. 5a ($R^2 = 0.924$). A favorable fit could be further certificated by the data as the calculated q_e value of pseudo-second-order model since it was extremely close to the measured one. Generally, the pseudo-second-order kinetics model was based on the assumption that the rate-limiting step related to chemisorption [5]. Accordingly, the adsorption process of TC onto NDMGO might involve chemisorption.

3.4. TC adsorption thermodynamics

To determine the influence of temperature on inherent energy change, thermodynamic experiments were explored at 283, 298,

Table 3
Thermodynamic parameters for TC adsorption by NDMGO.

T (K)	ln K_0	ΔG^o (kJ mol^{-1})	ΔH^o (J K^{-1} mol^{-1})	ΔS^o (kJ mol^{-1})
283	2.04	−4.81	31.17	0.013
298	2.48	−6.14		
313	3.31	−8.60		

and 313 K. The thermodynamic parameters involving standard free-energy change (ΔG^o), standard enthalpy change (ΔH^o), and standard entropy change (ΔS^o) are exhibited in the Supplementary materials (Table 3).

The negative value of ΔG^o suggested that the adsorption was a spontaneous adsorption process. The obtained value of ΔH^o was positive, which reflected the typical endothermic nature of adsorption reaction. It was consistent with the result that the adsorption capacity of TC increased along with the increase in temperature and higher temperature promoted the TC adsorption on NDMGO (Fig. 6). Besides, the positive value of ΔS^o implied the degrees of the randomness increased at the adsorbate-adsorbent interface. In solution, TC was surrounded by a tightly bound hydration layer where water molecules were more highly ordered than in the bulk water. When the TC molecules came into close interaction with the hydration surface of NDMGO, the ordered water molecules in these two hydration layers were compelled and disturbed, which would contribute to the increase of entropy. Although the adsorption of TC molecules on NDMGO surface caused the degree of freedom of TC molecules to decrease, it seemed likely that positive entropy related to the adsorption of TC on NDMGO was due to the entropy increase of water molecules overweighing the entropy decrease of TC molecules [47].

3.5. Effect of ionic strength

In general, industrial sewage contains high concentration of salts, and these salts can affect the adsorption of organic compounds [43]. Therefore, the effects of varying ionic strength
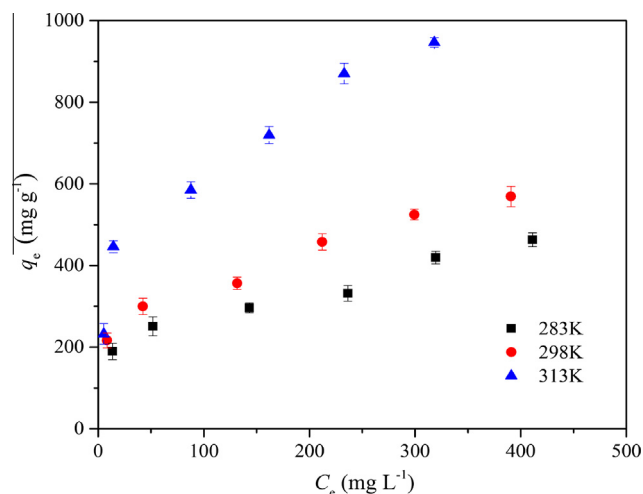

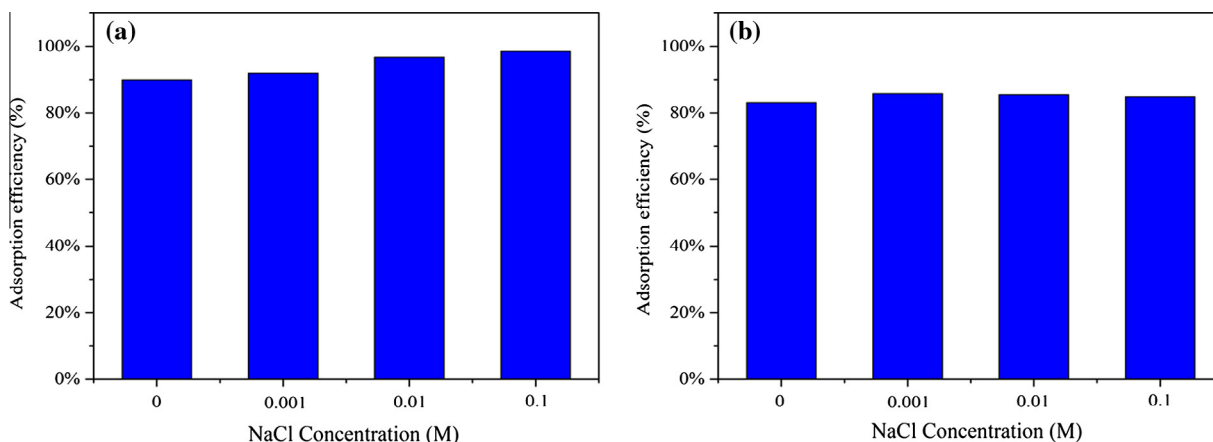**Fig. 6.** Effects of temperature on TC adsorption by NDMGO. $m/V = 0.19$ g L^{-1}, pH = 4.0, $t = 24$ h.

Fig. 7. Effects of ionic strength on TC adsorption by NDMGO at different initial concentrations of TC (a: 10 mg L^{-1}, b: 50 mg L^{-1}). m/V = 0.19 g L^{-1}, T = 25 °C, pH = 4.0, t = 24 h.
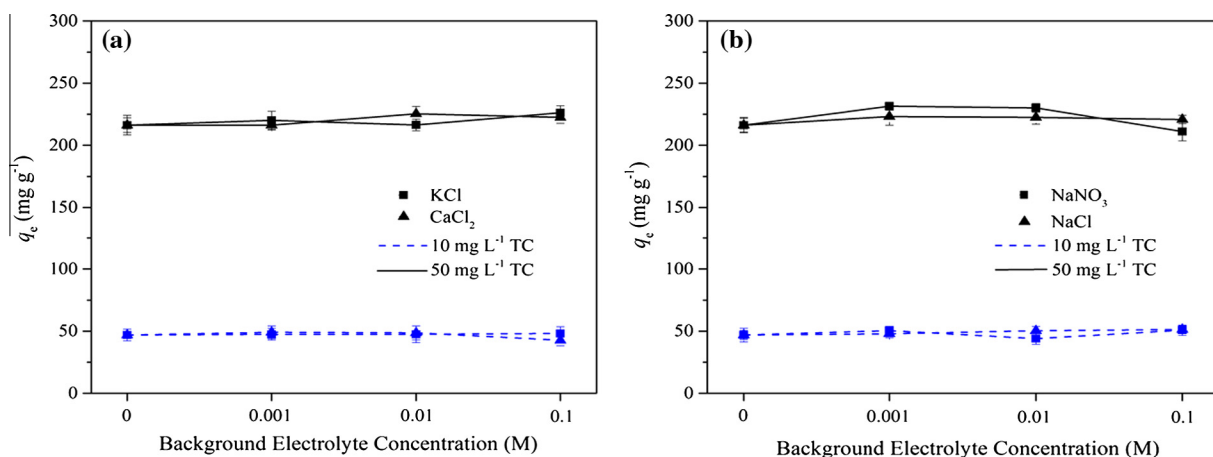

Fig. 8. Effects of background electrolytes on TC adsorption by NDMGO at different initial concentrations of TC. m/V = 0.19 g L^{-1}, T = 25 °C, pH = 4.0, t = 24 h.

(0.0–0.1 M) were studied. As shown in Fig. 7, it was found that the TC adsorption efficiency had a very limited raise with altering the concentration of NaCl. When the NaCl concentration was <0.01 M, the uptake of 10 and 50 mg L^{-1} TC increased with the increase of NaCl concentration. This phenomenon could be attributed to that the salt in solutions could enhance the activity coefficient of hydrophobic organic compounds (i.e. salting-out effect) and hence decreased the solubility of TC, resulting in promoting the TC adsorption on NDMGO [48]. The adsorption efficiency increased slightly when the NaCl concentration was >0.01 M. It indicated that the competition of Cl$^-$ with TC for the available binding sites was existed on NDMGO by a squeezing-out effect, and thus restricted the TC adsorption. Furthermore, this result also confirmed that the main adsorption force was not the surface electrostatic effects on the overall adsorption of TC on NDMGO.

3.6. Effect of background electrolytes

Fig. 8a and b shows the effects of foreign cations and anions such as K$^+$, Ca^{2+}, Cl$^-$ and NO$_3^-$ on the TC removal by NDMGO. Under two different TC concentrations, it was noticeable that the background electrolyte cations and anions had a negligible effect on TC removal from solutions. When the pH was 4.0, foreign cations in solutions could compete with the TC cations by a squeezing-out effect on the surface of oxidized NDMGO, but the competition of cations on TC adsorption by NDMGO were almost negligible with increasing

electrolyte concentration. This result might be contributed to the weak competitive nature of K$^+$ and Ca^{2+} as compared to TC cations for adsorption sites. Negatively charged anions might form complexes with the positively charged sites on the surface of NDMGO at pH 4.0, which could occupy the adsorption sites and thus were not conducive to remove TC. However, the TC adsorption on NDMGO was not influenced by the background electrolyte anions, suggesting that surface complexes were formed on NDMGO surface.

3.7. Desorption and regeneration evaluation

In the process of practical application, recycling capacity is regard as a crucial factor to evaluate the economy and applicability of adsorbents [49]. The results of desorption experiments are summarized in Fig. 9. After five regeneration cycles, the uptake capacity of TC on the recycling adsorbent still remained at 174 mg g^{-1}. The adsorption rate remained steady at about 78% in the five cycles compared with that of the first cycle, indicating that the NDMGO could be recycled for TC adsorption due to the excellent regeneration performance, which would effectively reduce the overall cost for the adsorbents.

3.8. Comparison with other adsorbents

The TC (initial concentration 150 mg L^{-1}) adsorption capacity by NDMGO obtained from the adsorption isotherm data (Fig. 6)
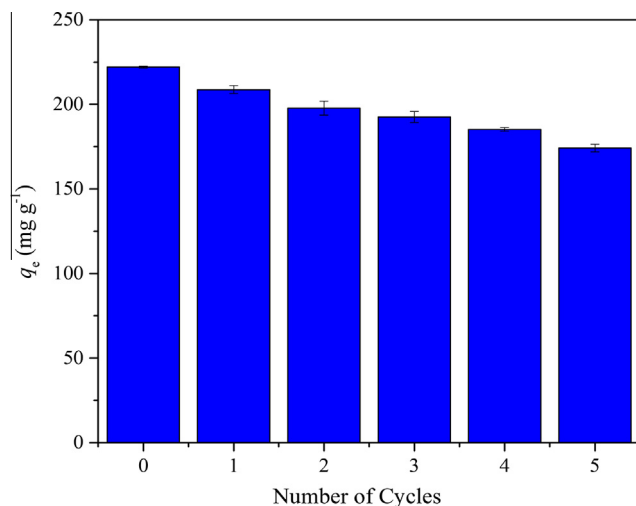
Fig. 9. Five adsorption-desorption cycles for NDMGO. $C_{0(TC)} = 50$ mg L^{-1}, $m/V = 0.19$ g L^{-1}, $T = 25$ °C, pH = 4.0, $t = 24$ h.

Fig. 10. FTIR spectra of NDMGO and TC after adsorption on NDMGO (NDMGO-TC).

was 356 mg g^{-1} at 298 K in this study, which showed a higher efficiency compared with the maximum adsorption of other adsorbents, such as GO (323 mg g^{-1}) [20], GO-MPs (39 mg g^{-1}) [50], MWCNTs (270 mg g^{-1}) [2], Fe/biochar (96 mg g^{-1}) [51]. Such comparison indicated that NDMGO might be an excellent adsorbent in treating TC wastewater.

3.9. Adsorption mechanism

In order to understand the interaction mechanism, the FT-IR and XPS studies were conducted. The FT-IR spectra of NDMGO and TC loaded NDMGO (NDMGO-TC complexes) are illustrate in Fig. 10.
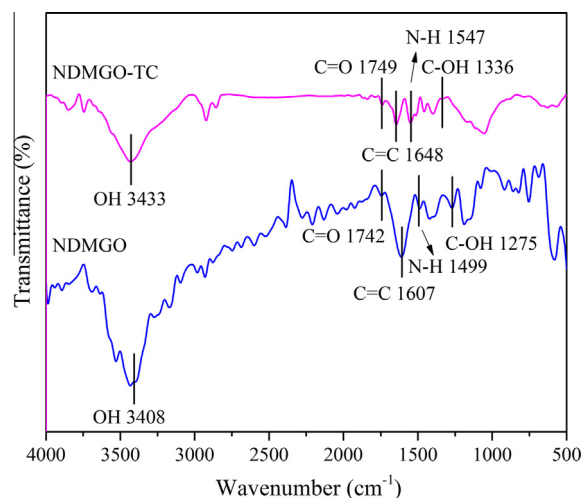
Several apparent characteristic peaks for NDMGO were observed at 1275, 1607, 1742, and 3408 cm^{-1}, resulting from the stretching vibration of the C—OH, C=C, C=O and O—H bonds, respectively [20,53]. After the adsorption of TC onto NDMGO, the peaks of C=C bonds presented a shift from 1607 to 1648 cm^{-1}, suggesting that the π-π interaction might be responsible for the significant changes [19]. Meanwhile, the easily protonated amino groups were located on the ring C_4 of the TC molecule, which could combine with the NDMGO or TC π-electrons. Besides, the N1s peak of XPS spectrum revealed the easily protonated amino groups were also existed in the grafted NTA-D, which could be bound with the NDMGO or TC π-electrons. So the cation-π bonding was likely to occur between protonated amino groups and π-electron-rich structures. The same mechanism was also observed by Ghadim
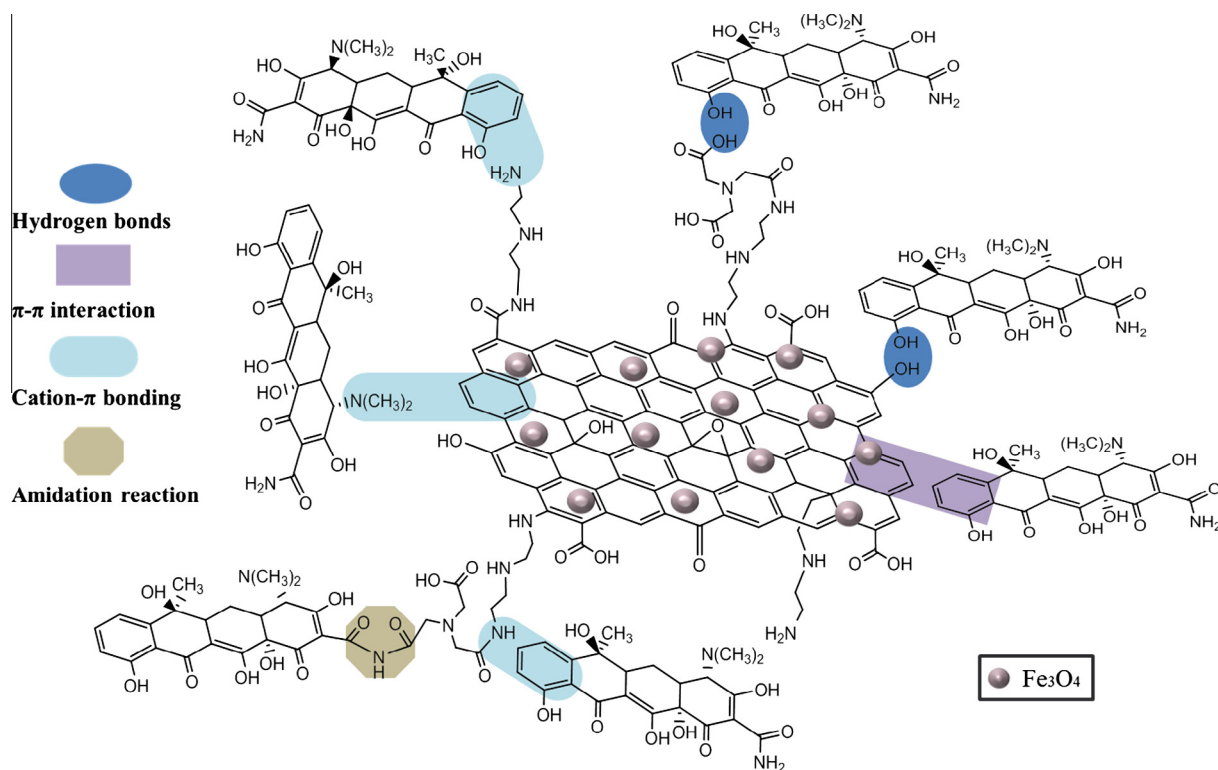

Fig. 11. Schematic illustration of adsorption mechanism by NDMGO.

et al. [20]. Compared with the NDMGO-TC complexes, the adsorption peak of NDMGO at 1742 and 3408 cm^{-1} belonged to the C=O bonds and O—H bending vibration migrated to 1749 and 3433 cm^{-1}, respectively, testifying that interactions between the oxygen-containing functional groups of NDMGO and TC molecules occurred, especially for —COOH and —OH [54]. Consequently, it was suggested that hydrogen bonds could also be used to elucidate the mechanism. Moreover, the characteristic signal of the secondary amide N—H bending shifted from 1499 to 1547 cm^{-1} [55], indicated that the amino-group probably played an important role in the TC uptake due to its strong chelating capability [56].

To further confirm these interaction mechanisms obtained from FT-IR analysis, XPS studies of NDMGO before and after the adsorption of TC were performed and the results are presented in Fig. 3 and Fig. S3. The C1s peaks before and after adsorption are shown in Fig. 3c and Fig. S3a, respectively. After TC uptake, the peak belonged to C—C/C=C group of NDMGO at 284.74 eV slightly shifted to 284.80 eV [39]. Meanwhile, from the N1s spectra in Fig. 3b and Fig. S3b, the peak of protonated amino groups shifted from 403.02 to 402.12 eV after adsorption [42,57]. The above results also gave strong evidence that the π-π interaction and cation-π bonding participated in the adsorption. The peak at 400.14 eV was attributed to the neutral and amine structure (—NH/C—N) [41], which had shifted to 400.52 eV after TC loaded onto NDMGO. In addition, for the C1s spectrum of NDMGO after adsorption (Fig. S3a), the peaks belonged to C—N and C=O groups at 285.50 and 286.35 eV shifted to 285.09 and 286.49 eV, respectively, indicated that newly formed amide bonds (—CO—NH—) played important roles in the NDMGO-TC complexes [41]. The O1s XPS spectra of NDMGO before and after adsorption are shown in Fig. S3c and d, respectively. The shift of the three peaks after TC adsorption might be due to the binding of amine and hydroxyl groups of TC onto the oxygen-containing functional groups of NDMGO or TC (The main oxygen-containing functional groups were hydroxyl and carboxyl groups) [44], proving that hydrogen bond probably presented in the adsorption process. The molecule interactions mechanism between NDMGO and TC are schematically illustrated in Fig. 11.

4. Conclusions

In this study, a novel magnetic absorbent was successfully synthesized by grafting NTA to MGO and developed for the removal of TC from aqueous solutions. The optimum pH condition of the adsorption of TC was 4.0. Owing to abundant amino and oxygen-containing groups, the adsorption ability of NDMGO was found to be two times higher to GO (109 mg g^{-1}) and three times higher to MGO (72 mg g^{-1}) when TC concentration was 50 mg L^{-1}. The pseudo-second-order kinetics model provided the better correlation for the experiment data. The TC adsorption followed a spontaneous and endothermic process. Ionic strength and foreign cations and anions within the typical ranges in natural waters had little effect on TC adsorption by NDMGO. Besides, NDMGO exhibited excellent regeneration performance by NaOH solution. Results also showed that hydrogen bonds, π-π interaction, cation-π bonding, and amidation reaction between NDMGO and TC might be the main adsorption mechanism.

The results obtained in this study suggested that the NDMGO was a high-efficiency and reusable adsorbent for TC removal from aqueous solutions. The optimal adsorption capacity occurred in weakly acidic environment. Compared to the maximum adsorption capacities of other adsorbents [2,51,52], the NDMGO had higher affinity for TC removal. Previous studies have shown that the GO-based composites could use to the removal of antibiotics [5,23,50]. This work improves our understanding of the interaction

mechanisms between the antibiotics and GO-based composites, and they are important for the environmental pollution control. Aspects of our continuing work should be included to study the influence of heavy metals (or other organics) on antibiotics adsorption and apply the NDMGO to treat actual medical wastewater in the future.

Appendix A. Supplementary material

Supplementary data associated with this article can be found, in the online version, at http://dx.doi.org/10.1016/j.jcis.2016.09.037.

References

[1] Y. Luo, L. Xu, M. Rysz, Y. Wang, H. Zhang, P.J. Alvarez, Occurrence and transport of tetracycline, sulfonamide, quinolone, and macrolide antibiotics in the Haihe River Basin, China, Environ. Sci. Technol. 45 (2011) 1827–1833.

[2] L. Zhang, X. Song, X. Liu, L. Yang, F. Pan, J. Lv, Studies on the removal of tetracycline by multi-walled carbon nanotubes, Chem. Eng. J. 178 (2011) 26–33.

[3] Y.J. Wang, D.A. Jia, R.J. Sun, H.W. Zhu, D.M. Zhou, Adsorption and cosorption of tetracycline and copper(II) on montmorillonite as affected by solution pH, Environ. Sci. Technol. 42 (2008) 3254–3259.

[4] H. Wang, N. Wang, B. Wang, Q. Zhao, H. Fang, C. Fu, C. Tang, F. Jiang, Y. Zhou, Y. Chen, Q. Jiang, Antibiotics in drinking water in Shanghai and their contribution to antibiotic exposure of school children, Environ. Sci. Technol. 50 (2016) 2692–2699.

[5] Y. Gao, Y. Li, L. Zhang, H. Huang, J. Hu, S.M. Shah, X. Su, Adsorption and removal of tetracycline antibiotics from aqueous solution by graphene oxide, J. Colloid Interface Sci. 368 (2012) 540–546.

[6] X. Huang, C. Liu, K. Li, J. Su, G. Zhu, L. Liu, Performance of vertical up-flow constructed wetlands on swine wastewater containing tetracyclines and tet genes, Water Res. 70 (2015) 109–117.

[7] J. Hou, C. Wang, D. Mao, Y. Luo, The occurrence and fate of tetracyclines in two pharmaceutical wastewater treatment plants of Northern China, Environ. Sci. Pollut. Res. Int. 23 (2016) 1722–1731.

[8] J. Giammarco, V.N. Mochalin, J. Haeckel, Y. Gogotsi, The adsorption of tetracycline and vancomycin onto nanodiamond with controlled release, J. Colloid Interface Sci. 468 (2016) 253–261.

[9] S. Kim, P. Eichhorn, J.N. Jensen, A.S. Weber, D.S. Aga, Removal of antibiotics in wastewater: effect of hydraulic and solid retention times on the fate of tetracycline in the activated sludge process, Environ. Sci. Technol. 39 (2005) 5816–5823.

[10] Y. Chen, C. Hu, J. Qu, M. Yang, Photodegradation of tetracycline and formation of reactive oxygen species in aqueous tetracycline solution under simulated sunlight irradiation, J. Photochem. Photobiol. A: Chem. 197 (2008) 81–87.

[11] A.K. Sarmah, M.T. Meyer, A.B. Boxall, A global perspective on the use, sales, exposure pathways, occurrence, fate and effects of veterinary antibiotics (VAs) in the environment, Chemosphere 65 (2006) 725–759.

[12] W.R. Chen, C.H. Huang, Adsorption and transformation of tetracycline antibiotics with aluminum oxide, Chemosphere 79 (2010) 779–785.

[13] R.A. Figueroa, A. Leonard, A.A. MacKay, Modeling tetracycline antibiotic sorption to clays, Environ. Sci. Technol. 38 (2004) 476–483.

[14] L. Ji, W. Chen, L. Duan, D. Zhu, Mechanisms for strong adsorption of tetracycline to carbon nanotubes: a comparative study using activated carbon and graphite as adsorbents, Environ. Sci. Technol. 43 (2009) 2322–2327.

[15] X.F. Tan, Y.G. Liu, G.M. Zeng, X. Wang, X.J. Hu, Y.L. Gu, Z.Z. Yang, Application of biochar for the removal of pollutants from aqueous solutions, Chemosphere 125 (2015) 70–85.

[16] X.F. Tan, Y.G. Liu, Y.L. Gu, Y. Xu, G.M. Zeng, X.J. Hu, S.B. Liu, X. Wang, S.M. Liu, J. Li, Biochar-based nano-composites for the decontamination of wastewater: a review, Bioresour. Technol. 212 (2016) 318–333.

[17] T. Hartono, S. Wang, Q. Ma, Z. Zhu, Layer structured graphite oxide as a novel adsorbent for humic acid removal from aqueous solution, J. Colloid Interface Sci. 333 (2009) 114–119.

[18] X. Chen, B. Chen, Macroscopic and spectroscopic investigations of the adsorption of nitroaromatic compounds on graphene oxide, reduced graphene oxide, and graphene nanosheets, Environ. Sci. Technol. 49 (2015) 6181–6189.

[19] J. Wang, Z. Chen, B. Chen, Adsorption of polycyclic aromatic hydrocarbons by graphene and graphene oxide nanosheets, Environ. Sci. Technol. 48 (2014) 4817–4825.

[20] E.E. Ghadim, F. Manouchehri, G. Soleimani, H. Hosseini, S. Kimiagar, S. Nafisi, Adsorption properties of tetracycline onto graphene oxide: equilibrium, kinetic and thermodynamic studies, PLoS ONE 8 (2013) 1–9.

[21] L. Ji, W. Chen, Z. Xu, S. Zheng, D. Zhu, Graphene nanosheets and graphite oxide as promising adsorbents for removal of organic contaminants from aqueous solution, J. Environ. Qual. 42 (2013) 191.

[22] S. Thiele Bruhn, Pharmaceutical antibiotic compounds in soils–a review, J. Plant Nutr. Soil Sci. 166 (2003) 145–167.

[23] L. Zhao, P. Dong, J. Xie, J. Li, L. Wu, S.T. Yang, J. Luo, Porous graphene oxide–chitosan aerogel for tetracycline removal, Mater. Res. Express 1 (2013) 015601.

[24] M. Liu, C. Chen, J. Hu, X. Wu, X. Wang, Synthesis of magnetite/graphene oxide composite and application for cobalt (II) removal, J. Phys. Chem. C 115 (2011) 25234–25240.

[25] H. Wang, Y.G. Liu, G.M. Zeng, X.J. Hu, X. Hu, T.T. Li, H.Y. Li, Y.Q. Wang, L.H. Jiang, Grafting of β-cyclodextrin to magnetic graphene oxide via ethylenediamine and application for Cr (VI) removal, Carbohydr. Polym. 113 (2014) 166–173.

[26] C.J. Madadrang, H.Y. Kim, G. Gao, N. Wang, J. Zhu, H. Feng, M. Gorring, M.L. Kasner, S. Hou, Adsorption behavior of EDTA-graphene oxide for Pb (II) removal, ACS Appl. Mater. Interfaces 4 (2012) 1186–1193.

[27] D. Wang, L. Liu, X. Jiang, J. Yu, X. Chen, Adsorption and removal of malachite green from aqueous solution using magnetic β-cyclodextrin-graphene oxide nanocomposites as adsorbents, Colloids Surf. A: Physicochem. Eng. Aspects 466 (2015) 166–173.

[28] F.Y. Guo, Y.G. Liu, H. Wang, G.M. Zeng, X.J. Hu, B.H. Zheng, T.T. Li, X.F. Tan, S.F. Wang, M.M. Zhang, Adsorption behavior of Cr(VI) from aqueous solution onto magnetic graphene oxide functionalized with 1,2-diaminocyclohexanetetraacetic acid, RSC Adv. 5 (2015) 45384–45392.

[29] S. Luo, X. Xu, G. Zhou, C. Liu, Y. Tang, Y. Liu, Amino siloxane oligomer-linked graphene oxide as an efficient adsorbent for removal of Pb(II) from wastewater, J. Hazard. Mater. 274 (2014) 145–155.

[30] G.K. Ramesha, A.V. Kumara, H.B. Muralidhara, S. Sampath, Graphene and graphene oxide as effective adsorbents toward anionic and cationic dyes, J. Colloid Interface Sci. 361 (2011) 270–277.

[31] L.H. Jiang, Y.G. Liu, G.M. Zeng, F.Y. Xiao, X.J. Hu, X. Hu, H. Wang, T.T. Li, L. Zhou, X.F. Tan, Removal of 17β-estradiol by few-layered graphene oxide nanosheets from aqueous solutions: external influence and adsorption mechanism, Chem. Eng. J. 284 (2016) 93–102.

[32] X.J. Hu, Y.G. Liu, H. Wang, A.W. Chen, G.M. Zeng, S.M. Liu, Y.M. Guo, X. Hu, T.T. Li, Y.Q. Wang, L. Zhou, S.H. Liu, Removal of Cu(II) ions from aqueous solution using sulfonated magnetic graphene oxide composite, Sep. Purif. Technol. 108 (2013) 189–195.

[33] Y. Lin, F. Lu, Y. Tu, Z. Ren, Glucose biosensors based on carbon nanotube nanoelectrode ensembles, Nano Lett. 4 (2004) 191–195.

[34] L. Fan, C. Luo, M. Sun, X. Li, H. Qiu, Highly selective adsorption of lead ions by water-dispersible magnetic chitosan/graphene oxide composites, Colloids Surf. B 103 (2013) 523–529.

[35] B. Huang, Y. Liu, B. Li, G. Zeng, X. Hu, B. Zheng, T. Li, L. Jiang, X. Tan, L. Zhou, Synthesis of graphene oxide decorated with core@double-shell nanoparticles and application for Cr(vi) removal, RSC Adv. 5 (2015) 106339–106349.

[36] N.A. Travlou, G.Z. Kyzas, N.K. Lazaridis, E.A. Deliyanni, Functionalization of graphite oxide with magnetic chitosan for the preparation of a nanocomposite dye adsorbent, Langmuir 29 (2013) 1657–1668.

[37] L.Z. Bai, D.L. Zhao, Y. Xu, J.M. Zhang, Y.L. Gao, L.Y. Zhao, J.T. Tang, Inductive heating property of graphene oxide–Fe$_3$O$_4$ nanoparticles hybrid in an AC magnetic field for localized hyperthermia, Mater. Lett. 68 (2012) 399–401.

[38] J. Ji, G. Zhang, H. Chen, S. Wang, G. Zhang, F. Zhang, X. Fan, Sulfonated graphene as water-tolerant solid acid catalyst, Chem. Sci. 2 (2011) 484–487.

[39] Z. Wu, H. Zhong, X. Yuan, H. Wang, L. Wang, X. Chen, G. Zeng, Y. Wu, Adsorptive removal of methylene blue by rhamnolipid-functionalized graphene oxide from wastewater, Water Res. 67 (2014) 330–344.

[40] R. Jansen, H. Van Bekkum, XPS of nitrogen-containing functional groups on activated carbon, Carbon 33 (1995) 1021–1027.

[41] Z. Zhang, S. Liu, M. Kang, G. Yang, Y. Li, F. Yan, L. He, X. Feng, P. Wang, S. Fang, Graphene nanostructures with plasma-polymerized pyrrole as an adsorbent layer for biosensors, Microchim. Acta 181 (2014) 1059–1067.

[42] Y.L. Yuan, F. Ai, J. Zhang, X.B. Zang, J. Shen, S.C. Lin, Grafting sulfobetaine monomer onto the segmented poly(ether-urethane) surface to improve hemocompatibility, J. Biomater. Sci. Polym. Ed. 13 (2002) 1081–1092.

[43] J. Xu, L. Wang, Y. Zhu, Decontamination of bisphenol A from aqueous solution by graphene adsorption, Langmuir 28 (2012) 8418–8425.

[44] S. Liu, H. Wang, L. Chai, M. Li, Effects of single- and multi-organic acid ligands on adsorption of copper by Fe$_3$O$_4$/graphene oxide-supported DCTA, J. Colloid Interface Sci. 478 (2016) 288–295.

[45] X. Ling, H. Li, H. Zha, C. He, J. Huang, Polar-modified post-cross-linked polystyrene and its adsorption towards salicylic acid from aqueous solution, Chem. Eng. J. 286 (2016) 400–407.

[46] H. Beheshti, M. Irani, L. Hosseini, A. Rahimi, M. Aliabadi, Removal of Cr (VI) from aqueous solutions using chitosan/MWCNT/Fe$_3$O$_4$ composite nanofibers-batch and column studies, Chem. Eng. J. 284 (2016) 557–564.

[47] G. Zhao, J. Li, X. Wang, Kinetic and thermodynamic study of 1-naphthol adsorption from aqueous solution to sulfonated graphene nanosheets, Chem. Eng. J. 173 (2011) 185–190.

[48] S. Zhang, T. Shao, S.S. Bekaroglu, T. Karanfil, Adsorption of synthetic organic chemicals by carbon nanotubes: effects of background solution chemistry, Water Res. 44 (2010) 2067–2074.

[49] L. Fan, C. Luo, Z. Lv, F. Lu, H. Qiu, Removal of Ag$^+$ from water environment using a novel magnetic thiourea-chitosan imprinted Ag$^+$, J. Hazard. Mater. 194 (2011) 193–201.

[50] Y. Lin, S. Xu, J. Li, Fast and highly efficient tetracyclines removal from environmental waters by graphene oxide functionalized magnetic particles, Chem. Eng. J. 225 (2013) 679–685.

[51] L. Peng, Y. Ren, J. Gu, P. Qin, Q. Zeng, J. Shao, M. Lei, L. Chai, Iron improving bio-char derived from microalgae on removal of tetracycline from aqueous system, Environ. Sci. Pollut. Res. 21 (2014) 7631–7640.

[52] R. Acosta, V. Fierro, A. Martinez de Yuso, D. Nabarlatz, A. Celzard, Tetracycline adsorption onto activated carbons produced by KOH activation of tyre pyrolysis char, Chemosphere 149 (2016) 168–176.

[53] Z. Fu, C. He, H. Li, C. Yan, L. Chen, J. Huang, Y.-N. Liu, A novel hydrophilic–hydrophobic magnetic interpenetrating polymer networks (IPNs) and its adsorption towards salicylic acid from aqueous solution, Chem. Eng. J. 279 (2015) 250–257.

[54] M. Nishio, CH/π-hydrogen bonds in crystals, ChemInform 35 (2004).

[55] Y. Lin, J. Jin, M. Song, Preparation and characterisation of covalent polymer functionalized graphene oxide, J. Mater. Chem. 21 (2011) 3455–3461.

[56] Z. Zhang, H. Liu, L. Wu, H. Lan, J. Qu, Preparation of amino-Fe(III) functionalized mesoporous silica for synergistic adsorption of tetracycline and copper, Chemosphere 138 (2015) 625–632.

[57] T. Chen, F. Liu, C. Ling, J. Gao, C. Xu, L. Li, A. Li, Insight into highly efficient coremoval of copper and p-nitrophenol by a newly synthesized polyamine chelating resin from aqueous media: competition and enhancement effect upon site recognition, Environ. Sci. Technol. 47 (2013) 13652–13660.